# Feasibility of Elemental Analysis of Kilogram-Size Samples by Instrumental Neutron Activation Analysis

**ARTICLE** *in* ANALYTICAL CHEMISTRY · JANUARY 1996

Impact Factor: 5.64 · DOI: 10.1021/ac950287w

CITATIONS
35

READS
19

**4 AUTHORS**, INCLUDING:

Ronald Overwater
National Institute for Public Health and the E…
**7** PUBLICATIONS **348** CITATIONS
SEE PROFILE

Peter Bode
Delft University of Technology
**151** PUBLICATIONS **2,259** CITATIONS
SEE PROFILE

Jan Eduard Hoogenboom
Delft University of Technology
**25** PUBLICATIONS **159** CITATIONS
SEE PROFILE

*Anal. Chem.* **1996,** *68,* 341−348

# Feasibility of Elemental Analysis of Kilogram-Size Samples by Instrumental Neutron Activation Analysis

Ronald M. W. Overwater,* Peter Bode, Jeroen J. M. de Goeij, and J. Eduard Hoogenboom

*Interfaculty Reactor Institute, Delft University of Technology, Mekelweg 15, 2629 JB Delft, The Netherlands*

**A method is presented that was neutron activation analysis for nondestructive multielement determinations in kilogram-size samples. Algorithms for correction of the neutron self-shielding and the $\gamma$-ray self-attenuation have been developed. These corrections do not require any a priori knowledge of the sample composition. The feasibility of the method has been validated by analyzing different 1−2-kg samples and comparing the results with those obtained from conventional small sample analyses of the same materials. Good agreement was observed. An outlook for future applications of kilogram-size sample analysis is given.**

Most analytical techniques deal with portions in the order of microliters to milliliters, and of milligrams to grams, whereas the amount of sampled material may easily be in the order of liters to kilograms, due to aspects of representativity and ease of operation.

Thus, it may be necessary to reduce the particle size of, to crush, to mill, and to homogenize the sample before the subsampling takes place; sometimes the material characteristics are such that homogenization to a representative sample of a few milligrams is almost impossible. Further, in all these processes, contamination and/or element loss may occur, while care is needed to avoid segregation. Finally, sample size reduction and homogenization "destroy" the originality of the sample taken.

Moreover, a method of elemental analysis that can handle analytical portions comparable in size to the samples initially taken, i.e., in the kilogram or liter range, may be attractive for particular applications. Trace element determinations in samples larger than the usual sizes mentioned above have been paid only limited attention in the analytical world. It is obvious that only the present day's nondestructive techniques have potential for such large samples. Of these techniques, instrumental neutron activation analysis (INAA) would be a method of choice, because of the high penetrating power of the neutrons used for activation and the $\gamma$-rays emitted by the activation products. At present, INAA is already used for bulk analyses, e.g., for well logging. On-line bulk analyses are also used in the industry for product, process, and supply control by using neutron generators. However, these applications are all customized to a specific problem, often aiming only at the major elements and with restrictions in standardization and universal applicability.

There are no physical limitations that would hamper the development of a routinely applicable form of INAA of very large samples with multielement determinations of state-of-the-art quantity and quality.[1] However, due to some serious complexities in the analysis, such a form of INAA has not yet been developed. In traditional INAA, the size of the analytical portion is so small that effects due to neutron self-shielding, neutron self-thermalization, and $\gamma$-ray attenuation can be neglected. All these effects cannot be ignored when dealing with large samples. Methods have to be developed to correct for neutron self-shielding during irradiation, for $\gamma$-ray attenuation during counting, and for the fact that the sample has such dimensions that it can no longer be represented as a point source during counting. For universal applicability, all these corrections should be performed using noninvasive techniques only.

At the Interfaculty Reactor Institute, a method is being developed for multielement INAA of kilogram-size samples. The maximum dimensions of the samples that can be handled in the facilities for irradiation and counting are 1 m in length, 15 cm in diameter, and ∼50 kg in mass. In this paper, the feasibility of the method for large sample INAA is shown by validation of the derived correction methods, viz., by comparing results from traditional small sample INAA and large sample INAA.

## FACILITIES

**Irradiation Facility.** A starting point in the development of large sample INAA has been that the amount of induced radioactivity should be of the same order of magnitude as for small sample INAA, not only to facilitate the handling and the counting of the sample but also to avoid the creation of a radioactive waste problem. Therefore, the larger the sample, the lower the desired neutron flux. Additionally, the aspect of neutron self-thermalization by, e.g., large quantities of hydrogen in the samples could be reduced by customizing the neutron spectrum to a high ratio of thermal over nonthermal neutron flux. The irradiation facility has been installed in the reactor's thermal column, which was fully filled with nuclear grade graphite blocks to obtain the desired low neutron flux and the well-thermalized spectrum. This irradiation facility is given the name BISNIS, which is an acronym for big sample neutron irradiation system.

In this irradiation facility, water is used as a shield against neutrons and $\gamma$-rays. A vertical cross section of the facility is depicted in Figure 1. The large sample is packed—surrounded by neutron flux monitors—in a polyethylene irradiation container. The flux monitors stay in a fixed position inside this container,

(1) In the traditional routine INAA at the Interfaculty Reactor Institute (Delft, The Netherlands), 200-mg samples are processed. Standardization of the ∼60 elements to be reported is based on the single-comparator method. The laboratory has been accredited for its quality system according to EN45001/ISO guide 25, see: Bode P.; van Dalen, J. P. J. *J. Radioanal. Nucl. Chem.* **1994**, *179*, 141−8.

0003-2700/96/0368-0341$12.00/0 

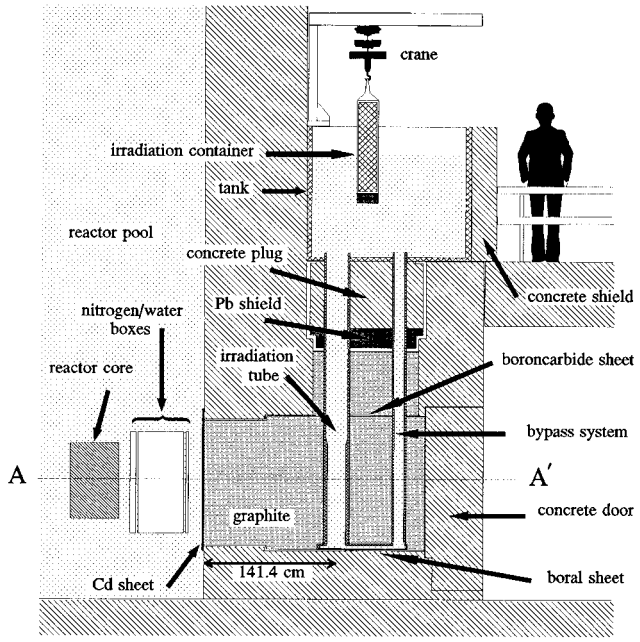


Figure 1. Schematic vertical cross section of the reactor's thermal column, showing the thermal column's irradiation facility.

while the sample is rotated around its vertical (length) axis during the irradiation.

**Counting Facility.** Measurement of the induced radioactivity is performed with a $\gamma$-ray spectrometer integrated in a scanning device. The $\gamma$-ray spectrometer includes a large volume HPGe semiconductor detector (relative efficiency 96% for the 1332 keV line of $^{60}$Co) and is linked to an HP/Apollo workstation of the laboratory's Local Area Network.[2] This workstation operates the scanner, too. The scanner allows for rotation around the vertical axis of the sample during counting and for vertical displacement with respect to the detector. By collimation of the detector, segmented scans can be performed, too.

## CORRECTION ALGORITHMS

**Neutrons.** In large sample INAA, corrections have to be applied for the neutron self-shielding. This self-shielding results in a lower neutron flux inside the sample than that expected on the basis of geometrical considerations alone. Measurement of the neutron flux distribution inside the sample by flux monitors was abandoned in concurrence with the wish for universal applicability. Attention was focused on calculation of the flux using as the only parameters the neutron diffusion length, $L$, and the neutron diffusion coefficient, $D$, of the sample. When all the major components of the voluminous sample's matrix are known, $L$ and $D$ of the entire sample can be calculated and therewith the neutron flux distribution inside the sample.

In most cases, however, the major components are not known. A way out is the phenomenon that the neutron flux is disturbed not only inside the sample but also outside the sample (the so-called neutron flux depression). This depression depends on the neutron absorbing and scattering properties of the sample and thus on $L$ and $D$. By measuring the neutron fluxes—by using flux monitors—just outside the sample, and with comparative values in a reference situation with a sample with well-known composition, the unknown $L$ and $D$ of the sample can be determined. To this end, an analytical solution of the neutron diffusion equation was derived for cylindrical samples in a two-dimensional geometry. The physics of this work has been described elsewhere.[3]

**$\gamma$-Rays.** In INAA-related $\gamma$-ray spectroscopy, two effects may, in principle, hamper correct evaluation of the peaks in the recorded spectrum of the activated voluminous sample: the intensity ratios between the various photopeaks are affected due to the energy dependency of the self-attenuation inside the sample, and the response of the detector is different for $\gamma$-rays emitted from different points from within the voluminous source.

A new, more general solution was developed for these two problems, although several approaches to account for these effects have been published in the past. As with the correction method for neutron self-shielding, no assumptions have been made with regard to size, shape, orientation, and composition of the sample.

The spatial effects due to measuring a voluminous sample instead of a more-or-less point source were solved by Monte Carlo calculations of the fate of a photon "generated" inside (and emitted by) the sample, until its final interaction with the detector. This approach included the correction for sample self-attenuation and requires experimentally determined linear attenuation coefficients of the sample as a function of the $\gamma$-ray energy and precise information on sample and detector dimensions. The linear attenuation coefficients of the large sample can easily be determined prior to activation by measuring the transmission of $\gamma$-rays from a standard source with well-known emission rates, and the detector dimensions are supplied by the manufacturer. The physics behind this correction method has been published elsewhere.[4]

**Combined Neutron and $\gamma$-Ray Attenuation.** When measuring the radioactivity of a neutron-activated large sample, an integral correction has to be applied, which combines the individual corrections described in the two previous sections. This integral correction method is based on a photon energy-dependent correction factor, $C$, by which the corresponding photopeak areas in the spectrum have to be multiplied to generate a $\gamma$-ray spectrum that would have been obtained had a small portion of that same material been analyzed. The correction factor for a cylindrical sample with the center at position $x_0,y_0,z_0$ (all in cm) relative to the detector end-cap and with its axis parallel to the $z$-axis (Figure 2) is defined as

$$C(E_\gamma,x_0,y_0,z_0,V) = \frac{\epsilon_{ps}(E_\gamma,x_0,y_0,z_0)}{\frac{1}{V}\int\int_V\int \epsilon_{ps}(E_\gamma,x,y,z)\ e^{-\mu(E_\gamma)\lambda(x,y,z)}\phi_{rel}(\varrho,z)\ dV} \quad (1)$$

In this equation, $\epsilon_{ps}(E_\gamma,x,y,z)$ is the efficiency of the detector in detecting a $\gamma$-ray with energy $E_\gamma$ emitted from a point source at a position $x,y,z$ (all in cm), $V$ is the volume of the voluminous source (cm$^3$), $\mu(E_\gamma)$ is the linear attenuation coefficient (cm$^{-1}$) of the sample for photons with energy $E_\gamma$, $\lambda(x,y,z)$ is the distance (cm) traveled by the photons inside the sample before leaving it, $\rho$ (cm)

(2) Blaauw, M.; Lindstrom, R. M. *J. Radioanal. Nucl. Chem.* **1993**, *169*, 443–52.

(3) Overwater, R. M. W.; Hoogenboom, J. E. *Nucl. Sci. Eng.* **1994**, *117*, 141–57.

(4) Overwater, R. M. W.; Bode, P.; de Goeij, J. J. M. *Nucl. Instrum. Methods* **1993**, *A324*, 209–18.

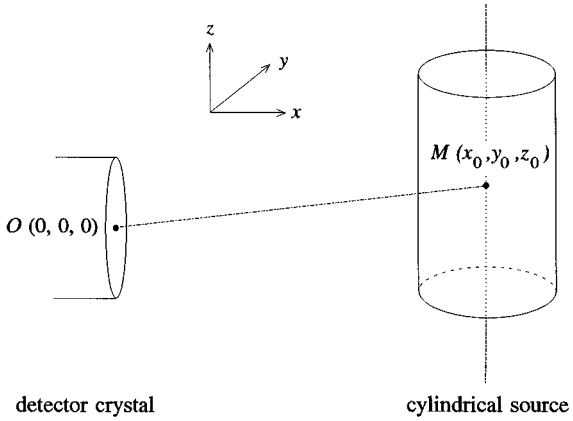


Figure 2. Position of the cylindrical source relative to the detector. The center of the detector surface is given the coordinates $O(0,0,0)$, and the center of the cylindrical source is given by the position $M(x_0,y_0,z_0)$.

is given by $\rho^2 = (x - x_0)^2 + (y - y_0)^2$, and the relative thermal neutron flux $\phi_{rel}(\rho,z)$ is given by the following equation:

$$\phi_{rel}(\rho,z) = \frac{\phi(\rho,z)}{\phi(\rho=R_s,z=z_0)} = \frac{\phi(\rho,z)}{\phi_0} \qquad (2)$$

In this expression, the averaging effect of rotation of the sample during irradiation on the neutron flux is used; the voluminous sample has thus virtually been irradiated with a corrected thermal neutron flux $\phi_0$ at the surface in the plane $z = z_0$. The calculation of the triple integral in the denominator of eq 1 is performed using the Monte Carlo method, as described elsewhere.[4] Multiplying the photopeak areas with this newly derived correction factor will correct for both neutron and $\gamma$-ray attenuation effects in the voluminous sample.

## EXPERIMENTAL SECTION

**Materials.** The materials were selected on basis of the following criteria: (1) a variety of long-lived radionuclides are produced during irradiation, (2) there are no visible inhomogeneities in the sample, (3) a wide range of atomic number and density is covered, and (4) the material is suitable for INAA. The following materials were selected: (a) coal fly ash, supplied by one of the nation's coal-fired power plants; (b) clay, taken from the Institute's premises; (c) phosphate ore from Jordan; raw product for the production of phosphoric acid and gypsum; and (d) a mixture of lamproite samples from Cabras, supplied by the Geological Museum in Amsterdam. From each of these four materials, one large sample and seven small subsamples were taken. The large sample was packed in a polyethylene bottle (diameter 9.4 cm, fill height 16.0 cm, volume 1 L, and masses of 1.04, 1.43, 1.63, and 2.02 kg, respectively), while the small samples were prepared by weighing 200−500 mg amounts in high-density polyethylene capsules (diameter 0.8 cm, height 1.0 cm). To avoid pressure buildup during irradiation, the small clay samples were freeze-dried. The large clay sample had not been dried; in the calculations, a correction was applied for the 33% moisture content of this material.

**Methods.** Each material passed the following standard procedure:

1. Measurement of the natural radioactivity of the large portion (corrected for background radiation) prior to irradiation.

2. Transmission measurement of the large portion using an external source prior to irradiation. This way, the linear attenuation coefficients are determined as a function of photon energy. Corrections have to be applied for both the natural radioactivity of the sample and the background radiation.

3. Measurement of the spectrum of the neutron-irradiated large portion, corrected for the natural radioactivity of the sample and the background radiation.

4. Calculation of the neutron parameters $L$ and $D$ and the thermal neutron flux $\phi_0$ for the large portion using the information from the external neutron flux monitors.

5. Calculation of the "calculated" correction factor, $C_{calc}$, for the irradiated large portion, using the results from steps 2 and 4.

6. Multiplication of the spectrum of the large portion (step 3) by the energy-dependent correction factor $C_{calc}$ (step 5). From here on, this corrected spectrum can be treated as a spectrum from a small sample, so the standard INAA procedures[1] can be used.

To validate large sample INAA based on calculated correction factors, the following additional steps were taken to check the correctness of the approach via these calculated correction factors:

7. Analysis of several small portions, according to the traditional INAA routine procedure; in this procedure the $\gamma$-ray spectrum is measured and corrected for background radiation.

8. Calculation of the "measured" correction factor, $C_{meas}$, using the results from steps 3 and 7. Corrections have to be applied for differences in irradiation, decay, and measuring times and for differences in thermal neutron flux and sample masses.

9. Comparison between the measured and calculated correction factors.

**Homogeneity Tests.** The homogeneity of the materials was tested, analyzing seven small subsamples with standard INAA. Every analysis of a subsample results in a list of elements and concentrations. All seven lists of concentrations were averaged per element, resulting in an average concentration with a standard error of the mean.

**$\gamma$-Ray Linear Attenuation Coefficients.** The transmission measurements are performed before irradiation in order to avoid interference between the induced radioactivity in the sample and $\gamma$-ray lines from the transmission source containing 23 kBq of $^{152}$Eu and 4.8 kBq of $^{22}$Na. Interferences with lines from the natural radioactivity of the sample and the background around the counting facility cannot be avoided, and therefore both were measured, too, and used to correct the transmission spectra with.

**Irradiation Conditions.** The small samples were irradiated as follows: Each of the seven small samples was paired with a flux monitor (2 mg of metallic zinc). The seven pairs were stacked in two columns, one containing four samples, the other containing three samples. These columns, wrapped in heat-sealed plastic foil, were packed in a high density polyethylene container (diameter 4.0 cm, length 15.0 cm), to be irradiated for 1 h in the BP3 pneumatic irradiation facility of the Hoger Onderwijs Reactor of the Interfaculty Reactor Institute. The irradiation end of this facility is located aside the reactor core in the water reflector. The total neutron flux in this facility is in the order of $5 \times 10^{12}$ cm$^{-2}$ s$^{-1}$, while the ratio of thermal to epithermal neutron flux is ~40.

The large samples were irradiated as follows: Each large sample was coupled with 16 flux monitors (each 70 mg of metallic zinc). The large sample, packed in a polyethylene bottle, was wrapped in heat-sealed plastic foil, and subsequently packed in a

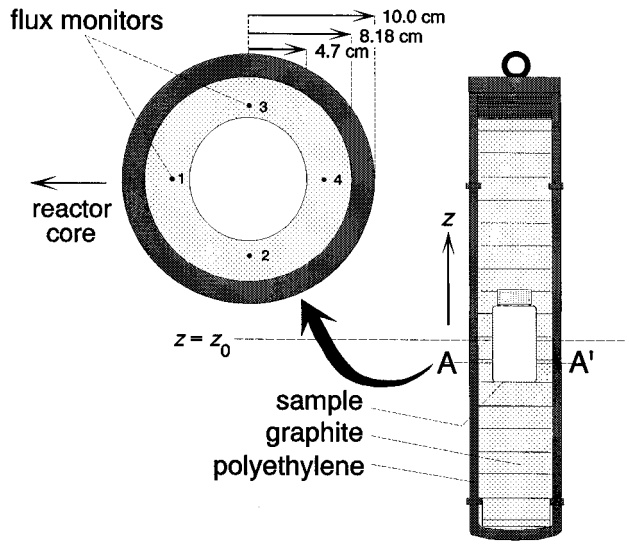


Figure 3. Irradiation container as filled during irradiations. The filling of a layer in which the sample is present is shown on the left.

polyethylene irradiation container (diameter 20 cm, length 100 cm); the remaining void in the container was filled with nuclear-grade graphite. In this container, the sample was surrounded by the 16 flux monitors (four different layers with four flux monitors each), as can be seen in Figure 3. This container was then irradiated for 24 h in the BISNIS irradiation facility. The total neutron flux in this facility is in the order of $2.5 \times 10^8$ cm$^{-2}$ s$^{-1}$, while the ratio of thermal to nonthermal neutron flux is calculated to be ~250.

**Neutron Flux and Neutron Parameters.** The theory developed to correct for the neutron self-shielding is limited to two dimensions and assumes an infinite size in the third dimension. Due to the fact that the sample is limited in height, *z*-dependence of the flux in the sample can be expected. Therefore, both the diffusion length and the diffusion coefficient are determined as a function of *z*, through flux measurements at different heights along the sample. These flux measurements include measurements for both the sample of interest and a reference sample. The reference flux also shows a *z*-dependence. The function $\phi(\rho,z)$ depicts the *z*-dependence and is numerically evaluated through interpolation between calculated fluxes at the different measured heights in the sample, using the fitted $L(z)$ and $D(z)$ as well as the absolute reference flux for each height.

The errors in the fitted $L$ and $D$ values—resulting from statistical errors in the measured flux depressions—have been propagated into the calculation of the correction factor.

**Measured Correction Factor ($C_{meas}$).** A brief introduction of some of the formulas used in the quantification in INAA[5] clarifies the approach for determining the correction factor as the ratio of the efficiency of a point source, $\epsilon_{ps}$, to that of a voluminous source, $\epsilon_{vs}$, by comparing the measured spectra of both sources.

The probability $R$ of a nucleus having an $(n,\gamma)$ reaction in a unit of time (s$^{-1}$) during irradiation is given by

$$R = \phi_{th}\sigma_0 + \phi_{epi}I_0 = \phi_{th}\sigma_0(1 + Q_0/f) \qquad (3)$$

where $\phi_{th}$ is the thermal neutron flux, $\phi_{epi}$ is the epithermal neutron flux, $\sigma_0$ is the thermal neutron $(n,\gamma)$ cross section, $I_0$ is the epithermal neutron $(n,\gamma)$ resonance integral, $Q_0$ is given by $Q_0 = I_0/\sigma_0$, and $f$ is given by $f = \phi_{th}/\phi_{epi}$.

The number of activated nuclei in a sample disintegrating during the measurement, $\Delta N$, after an irradiation time $t_{ir}$, a decay time $t_d$, and a counting time $t_c$, is given by

$$\Delta N = R\frac{\theta N_{Avo} w}{\lambda M} G_S G_D G_C \qquad (4)$$

where $\theta$ is the isotopic abundance of the isotope of interest, $N_{Avo}$ is Avogadro's number (mol$^{-1}$), $w$ is the amount of element (g), $\lambda$ is the probability of disintegration per unit time (s$^{-1}$), $M$ is the atomic mass (g mol$^{-1}$), $G_S = 1 - e^{-\lambda t_{ir}}$ is the saturation correction, $G_D = e^{-\lambda t_d}$ is the decay correction, and $G_C = 1 - e^{-\lambda t_c}$ is the counting correction.

The area $A$ of the so-called photopeak for a given photon energy $E_\gamma$ in the spectrum, assuming no summation, is given by

$$A = \gamma\epsilon\Delta N \qquad (5)$$

where $\gamma$ is the absolute $\gamma$-ray abundance, i.e., the probability of the disintegrating nucleus emitting a photon of this energy, and $\epsilon$ is the absolute photopeak efficiency of the detector, being either $\epsilon_{ps}$ or $\epsilon_{vs}$ (cf. eq 1). For the voluminous source, $\epsilon_{vs}$ also includes the self-attenuation of neutrons during irradiation.

The concentration $K$ of the element in the sample (g/g) is given by

$$K = \frac{w}{m} = \frac{\lambda M}{\gamma\theta N_{Avo}} \frac{A}{mR\epsilon G_S G_D G_C} \qquad (6)$$

where $m$ is the mass of the sample (g).

If the material from which both the small and the large samples are taken is homogeneous, the concentrations for both the small sample and the large sample must be the same:

$$\frac{A_{ps}}{m_{ps}R_{ps}\epsilon_{ps}G_{S,ps}G_{D,ps}G_{C,ps}} = \frac{A_{vs}}{m_{vs}R_{vs}\epsilon_{vs}G_{S,vs}G_{D,vs}G_{C,vs}} \qquad (7)$$

resulting in, using the definition of the correction factor $C_{meas}$,

$$C_{meas} \equiv \frac{\epsilon_{ps}}{\epsilon_{vs}} = \frac{A_{ps}m_{vs}R_{vs}G_{S,vs}G_{D,vs}G_{C,vs}}{A_{vs}m_{ps}R_{ps}G_{S,ps}G_{D,ps}G_{C,ps}} \qquad (8)$$

This correction factor is still a function of the $\gamma$-ray energy $E_\gamma$ and has been calculated for all photopeak energies of interest.

**Calculated Correction Factor ($C_{calc}$).** The correction factor $C(E_\gamma,x_0,y_0,z_0,V)$, as given in eq 1, is based on the results obtained by the transmission measurement and the measurements of the neutron flux depression.

The errors in the values of $\mu(E_\gamma)$, the strongly correlated $L(z)$ and $D(z)$, $\phi(\rho{=}R_s,z)$, and $\phi_0$ are all included in the calculation of the total error in the correction factor, thereby making a distinction between systematic and statistical errors. The error in $\mu(E_\gamma)$ is a statistical error, due to counting statistics, and can be different for every value of $E_\gamma$. The other errors are almost independent

(5) Ehmann, W. D.; Vance, D. E. *Radiochemistry and Nuclear Methods of Analysis*; John Wiley & Son, Inc.: New York, 1991; Chapter 9.

Table 1. Average Concentrations of the Trace Elements Found in the Four Materials Studied[a]

| element | coal fly ash | clay | phosphate ore | lamproite rock |
|---|---|---|---|---|
| Na | 2290 (0.9) | 4990 (0.6) | 3720 (1.4) | 7490 (0.6) |
| K | 9376 (5.8) | 15650 (2.0) | | 72710 (1.1) |
| Ca | | 43180 (5.6) | | 378600 (1.2) |
| Sc | 29.3 (0.2) | 9.17 (0.3) | 1.47 (1.0) | 13.6 (0.4) |
| Cr | 54.1 (2.8) | 83.4 (1.7) | 67.7 (2.1) | 743 (0.7) |
| Fe | 39570 (0.6) | 28180 (0.7) | 1170 (14) | 36650 (0.9) |
| Co | 54.2 (0.8) | 8.83 (2.2) | | 36.7 (1.5) |
| Ni | | | | 479 (10) |
| Zn | 183 (5.7) | 96 (8.7) | 120 (8.6) | |
| As | 17.7 (1.7) | 13.2 (1.1) | 5.56 (1.9) | 8.15 (2.4) |
| Br | 2.57 (5.5) | 24.6 (0.5) | 1.98 (2.8) | |
| Rb | | 88.5 (5.7) | | 574 (2.1) |
| Sb | 5.96 (1.0) | 0.83 (3.2) | 0.37 (5.2) | |
| Cs | 6.62 (2.9) | 8.08 (1.8) | | 23.0 (1.4) |
| Ba | 502 (10) | 291 (6.7) | | 1400 (5.6) |
| La | 58.2 (0.2) | 26.3 (0.2) | 16.3 (0.4) | 108 (0.2) |
| Ce | 134 (1.6) | 53.3 (2.0) | 23.8 (4.7) | 315 (1.1) |
| Sm | 13.2 (0.2) | 4.60 (0.4) | 1.69 (2.9) | 30.3 (0.2) |
| Eu | 2.78 (1.4) | 1.00 (2.7) | 0.59 (7.9) | 5.67 (2.3) |
| Tb | 2.39 (2.8) | 0.56 (14) | 0.53 (19) | |
| Yb | 9.75 (0.6) | 2.14 (1.5) | 1.75 (1.9) | 1.89 (2.9) |
| Lu | 1.58 (1.2) | 0.34 (2.4) | 0.31 (13) | 0.22 (9.8) |
| Hf | 16.7 (1.1) | 6.61 (1.7) | | 24.1 (1.2) |
| W | 6.65 (5.0) | | | 3.57 (7.7) |
| Th | 23.5 (0.9) | 9.19 (1.3) | 1.39 (8.8) | 125 (0.4) |
| U | 6.54 (1.7) | 1.96 (3.6) | 46.6 (0.4) | 15.4 (1.1) |

[a] The values are the average (in mg/kg) for all seven small samples, and the errors in parentheses are standard errors of the mean (SEM, %).

of the $\gamma$-ray energy $E_\gamma$ and result in an equal error for all correction factors, which is therefore said to be systematic.

## RESULTS

**Homogeneity.** Since none of the concentrations appeared to deviate more than two standard deviations from the mean concentration of a particular element, the degree of elemental homogeneity of all four materials is taken as sufficient for this application. The mean concentrations and their errors for all four materials is given in Table 1.

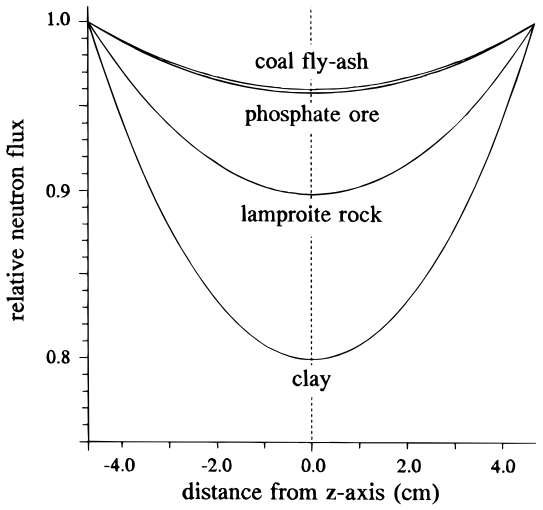


Figure 4. Results of the relative neutron flux $\phi_{rel}(\rho,z)$ for all four large samples.

**Neutron Self-Shielding.** The neutron parameters $L$ and $D$ were determined at different heights inside the voluminous sample. The values for $\phi_0 = \phi(\rho = R_s, z = z_0)$ are found by a fourth-order polynomial interpolation. The results are given in Table 2 and Figure 4.

The limited neutron absorption and scattering of coal fly ash and phosphate ore result in an almost flat neutron flux profile inside the sample. The decrease of the neutron flux in the clay material is much more pronounced due to the large amount of water in the sample. It is assumed that the decrease in neutron flux in the lamproite sample results from significant amounts of trace elements with a high neutron absorption cross section, such as 800 mg/kg Mn.

**$\gamma$-Ray Linear Attenuation Coefficients.** The transmission beam is not a perfect pencil beam; therefore, the average distance traveled through the sample was calculated using the Monte Carlo program. For a pencil beam, the distance traversed through the sample equals the diameter of the sample (9.4 cm), while for the

Table 2. Neutron Parameters $D(z - z_0)$ and $L(z - z_0)$, and Flux $\phi(\rho = R_s, z - z_0)$ Found by Fitting External Flux Monitors for the Four Materials Studied[a]

| material | $z - z_0$ (cm) | $\phi(\rho = R_s, z - z_0)$ ($10^8$ cm$^{-2}$ s$^{-1}$) | $L$ (cm) | $\Delta L$ (cm) | $D$ (cm) | $\Delta D$ (cm) |
|---|---|---|---|---|---|---|
| coal fly ash | −3.5 | 2.39 | 10.96 | 0.92 | 2.00 | 0.36 |
| | 0.0 | 2.36 | | | | |
| | 1.5 | 2.36 | 11.61 | 1.00 | 2.18 | 0.40 |
| | 6.5 | 2.41 | 11.27 | 0.91 | 1.76 | 0.31 |
| | 11.5 | 2.45 | 11.50 | 0.89 | 1.55 | 0.26 |
| clay | −3.5 | 2.24 | 5.38 | 0.46 | 0.59 | 0.10 |
| | 0.0 | 2.20 | | | | |
| | 1.5 | 2.20 | 4.84 | 0.45 | 0.51 | 0.09 |
| | 6.5 | 2.27 | 5.52 | 0.47 | 0.55 | 0.09 |
| | 11.5 | 2.30 | 7.98 | 0.59 | 0.95 | 0.15 |
| phosphate ore | −3.5 | 2.44 | 10.35 | 0.85 | 1.66 | 0.28 |
| | 0.0 | 2.41 | | | | |
| | 1.5 | 2.41 | 11.31 | 0.98 | 1.57 | 0.35 |
| | 6.5 | 2.45 | 10.70 | 0.81 | 1.44 | 0.23 |
| | 11.5 | 2.46 | 11.74 | 0.89 | 1.52 | 0.24 |
| lamproite rock | −3.5 | 2.07 | 7.05 | 0.60 | 1.37 | 0.23 |
| | 0.0 | 2.02 | | | | |
| | 1.5 | 2.02 | 7.07 | 0.61 | 1.44 | 0.25 |
| | 6.5 | 2.13 | 7.71 | 0.64 | 1.35 | 0.23 |
| | 11.5 | 2.28 | 9.29 | 0.70 | 1.26 | 0.20 |

[a] The values for $z - z_0 = 0$ are interpolated values, and therefore no $L$ and $D$ are found in those cases.

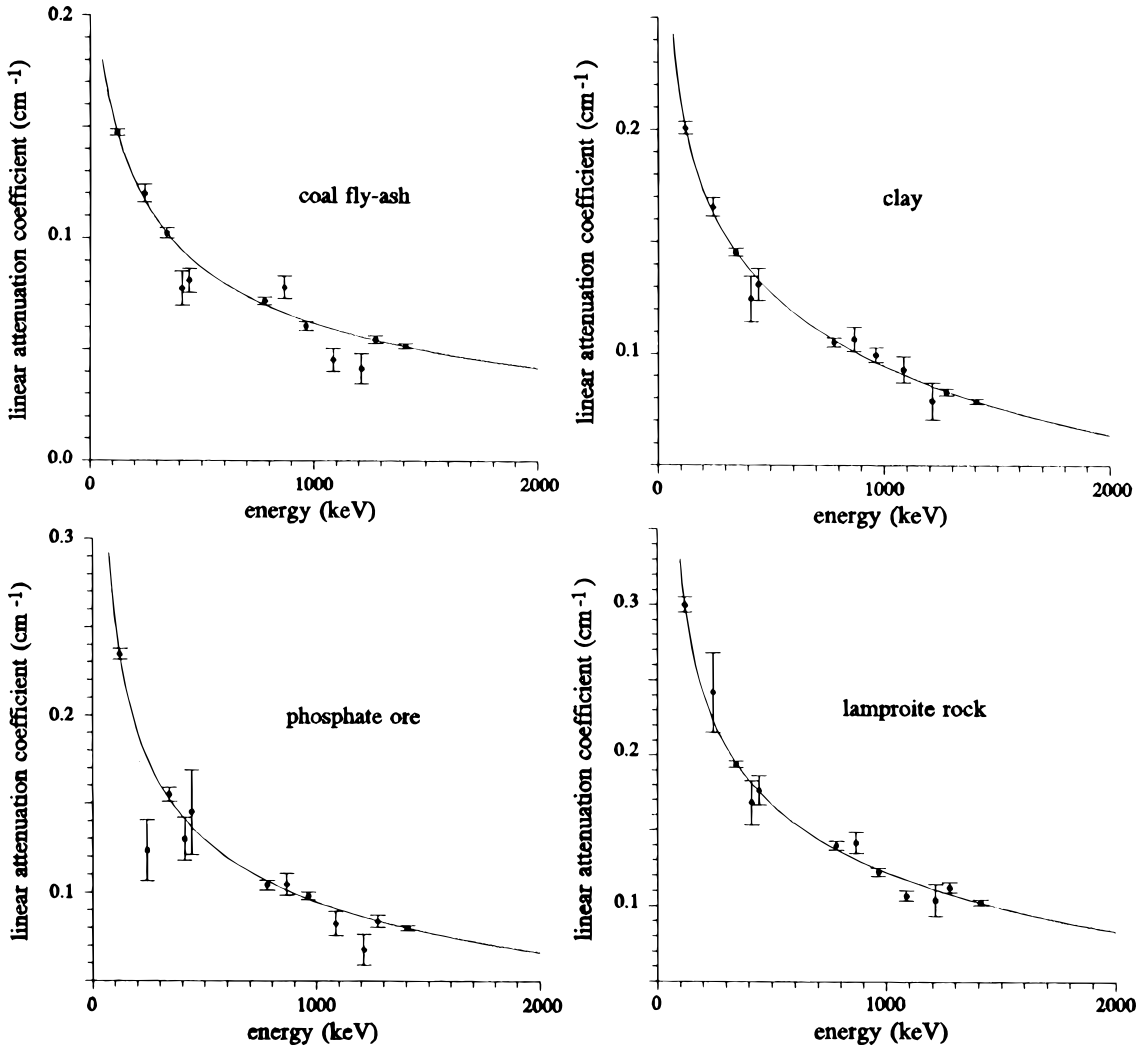


Figure 5. Results of the linear attenuation coefficient $\mu(E_\gamma)$ for all four large samples. The solid line (a third-order log−log fit) is shown here to guide the eye.

real beam, the average distance traveled through the sample is ~9.3 cm (still dependent on the $\gamma$-ray energy).

The measured linear attenuation coefficients at the photopeak energies emitted by the mixed $^{152}$Eu−$^{22}$Na source are shown in Figure 5. The measured data points have been fitted with a third-order log−log polynomial. All data points are within two standard deviations from the fitted curve, except for the point derived from the 244 keV transmission in the phosphate ore sample. A strong interference due to the 242 keV line of the $^{214}$Pb daughter of the naturally occurring $^{226}$Ra results in poor precision of this data point.

**Measured Correction Factor ($C_{meas}$).** Only interference-free $\gamma$-ray lines can be used to calculate $C_{meas}$. This results in the following radionuclides and lines: $^{24}$Na (1369 keV), $^{42}$K (1525 keV), $^{46}$Sc (889 and 1120 keV), $^{47}$Sc (159 keV), $^{51}$Cr (320 keV), $^{140}$La (329, 432, 487, 752, 815, 867, 925, and 1596 keV), $^{152m}$Eu (841 and 1408 keV), $^{153}$Sm (103 keV), $^{175}$Yb (396 keV), and $^{239}$Np (106 and 277 keV). In addition, a photopeak is excluded from the calculations when the statistical error in the photopeak area measured exceeds 20%.

The parameters $\sigma_0$, $I_0$, and $\lambda$ were derived from the literature,[6] and the values for $f$ are given in the section Irradiation Conditions.

(6) Glascock, M. D. *Tables for Neutron Activation Analysis*; University of Missouri: Colombia, MO, 1988.

The results of the measured correction factors are given in Figure 6. The statistical error in the measured correction factor is due to the statistical errors in $A_{ps}$ and $A_{vs}$ only. The systematic errors in the measured correction factors are due to the errors in both $\phi_{th,ps}$ and $\phi_{th,vs}$ (~1.5% each) and also due to imperfect positioning of both samples (~0.5%).

**Calculated Correction Factor ($C_{calc}$).** The correction factor $C_{calc}$ is calculated by performing a Monte Carlo computation, using the results for $\mu(E_\gamma)$, $L(z)$, $D(z)$, $\phi(\rho = R_s,z)$, and $\phi_0$. This calculation is done for each of the $\gamma$-ray energies used in the measurement of $\mu(E_\gamma)$. For each material, these 12 correction factors are then fitted to a third-order log−log polynomial function of the $\gamma$-ray energy. The resulting curves are shown in Figure 6.

The statistical errors in the correction factors determine the inaccuracy of the resulting fit. The inaccuracy in the fit is so small that deviations are visible only if the curve is extrapolated far beyond the outermost energies (122 and 1408 keV). Thus, there is no significant statistical error in the calculated correction factor fit for the $\gamma$-ray energies of interest in this study. However, there is a systematic error due to systematic errors in $L(z)$ and $D(z)$, resulting in errors of 0.3%, 1.3%, 0.3%, and 0.7%, for materials 1−4, respectively. These systematic errors are represented, together

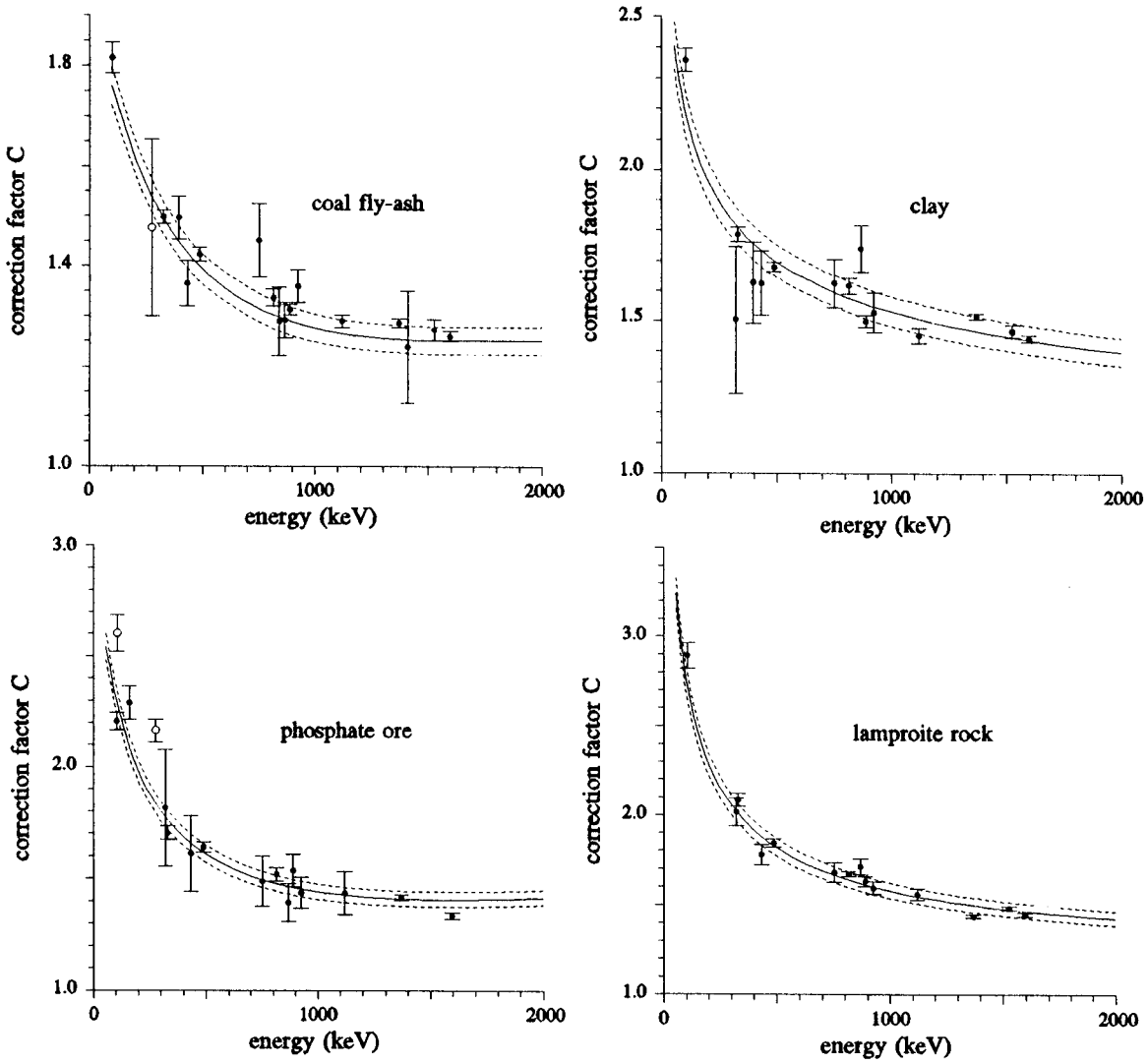


Figure 6. Results of the measured and calculated correction factors $C(E_\gamma,x_0,y_0,z_0,V)$ for all four large samples. The dashed lines represent the $1\sigma$ systematic error bands.

with those of the previous section, by the dashed lines ($1\sigma$ bands) in Figure 6.

**Comparison of Calculated and Measured Correction Factors.** Because the calculated and measured correction factors are not calculated and/or measured at the same energies, a comparison was made between the measured correction factor and the calculated correction factor by using the third-order log−log fit described in the previous section. To quantify the deviation between the measured and the calculated correction factors per material, $\chi^2$ is defined here by

$$\chi^2(F) = \frac{1}{N}\sum_{i=1}^{N}\left[\frac{FC_{\mathrm{calc}}(E_i) - C_{\mathrm{meas}}(E_i)}{\Delta C(E_i)}\right]^2 \qquad (9)$$

where $E_i$ is the energy of the data point, $N$ is the number of data points used, $F$ is a multiplication factor used to account for systematic errors, and $\Delta C$ is the combined statistical error of the measured and the calculated correction factors, given by

$$\Delta C = \sqrt{(\Delta C_{\mathrm{meas}})^2 + (F\Delta C_{\mathrm{calc}})^2} \approx \Delta C_{\mathrm{meas}} \qquad (10)$$

The last approximation is justified, since the statistical error in the fit of the calculated correction factors can be neglected compared to the statistical error in the measured correction factors. The exact location of the fitted curve is not yet fixed due to possible systematic errors but most probably will lie between the two dashed lines in Figure 6. The $F$ value describes the factor by which $C_{\mathrm{calc}}$ has to be multiplied for a more optimal match to $C_{\mathrm{meas}}$. A $\chi^2$ nearly equal to 1.0 indicates that the spread in the data points is well explained (for $N = 15$ and $\alpha = 0.05$, $0.42 < \chi^2 < 1.74$).

Since the value of $f = 250$ (cf eq 3) for the BISNIS irradiation facility is only a purely theoretical one, the result of the measured correction factor for $^{238}$U (see the open circles in Figure 6) may be much more inaccurate than the statistical error flags show.

Table 3. Quality Parameters $\chi^2(F)$ and $F^a$ for $N$ Different Energies for the Four Materials Studied

| | coal fly ash | clay | phosphate ore | lamproite rock |
|---|---|---|---|---|
| $N$ | 16 | 15 | 14 | 14 |
| $\chi^2(F)$ | 1.13 | 4.63 | 3.17 | 4.50 |
| $F$ | 1.017 | 1.007 | 0.988 | 0.995 |

[a] As defined in the section Comparison of Calculated and Measured Correction Factors.

This is due to a high $Q_0$ of $^{238}U$ ($\sim$100), indicating a high sensitivity for inaccuracy in this $f$. Therefore, the $^{238}U$ values are not used in the calculation of $\chi^2$.

$\chi^2(F)$ was minimized to find the value of $F$ for which $\chi^2(F)$ has a minimum value. A "perfect" match between theory and measurement is obtained if $F$ is such that the shifted fitted curve falls between the dashed 1$\sigma$ error lines. The results are given in Table 3.

## DISCUSSION

Since the correction factor $C$ is merely determined by the effects of the $\gamma$-ray self-attenuation, at least with the samples studied here, large uncertainties in $L$—and herewith strongly correlated large uncertainties in $D$—do not necessarily imply large errors in this factor. The situation for material 2 (clay) is quite different from that for material 1 (coal fly ash), due to the much smaller diffusion length of material 2. It turned out that for $L >$ 10 cm, rotation of the large sample results in an almost flat flux profile and consequently small errors in $C$, due to the neutron flux parameters. This applies to material 1, but not to material 2.

The comparison of calculated and measured correction factors shows an overall good agreement ($F$ values) for all four materials (Table 3), well within the systematic 1$\sigma$ error bands shown in Figure 6. The results for materials 2−4 show a high $\chi^2$, indicating that the experiment was statistically not completely under control. These high values are due mainly to only two or three data points, which are off by more than three standard deviations. For material 2 (clay), both measured correction factors of $^{46}Sc$ show the same absolute deviation from the fitted calculated correction factor: they are both 6% too low (the same holds true for $^{24}Na$). Although the small subsamples showed good homogeneity among themselves, the subsamples probably are not representative enough for the large sample. For material 4 (lamproite rock), insufficient representativity of the small samples may explain the deviation for $^{24}Na$, the only measured correction factor off by more than three standard deviations. The deviation for the measured correction factor at the 1596 keV line of $^{140}La$ for material 3 (phosphate ore) is probably an artifact, because all other measured correction factors of $^{140}La$ fit on the calculated correction factor curve.

The validation experiments show that the $\gamma$-ray attenuation dominates the neutron attenuation in the sample types studied, which may be considered typical for INAA. For diffusion lengths as small as 5 cm (claylike material) and linear attenuation coefficients as large as 0.3 $cm^{-1}$ (122 keV $\gamma$-rays in lamproite rock), corrections can be performed on 1−2 kg samples with only a small loss in accuracy as compared to routinely applied INAA for small samples.

## OUTLOOK

This study has demonstrated that large sample analysis is well feasible. Applications of large sample INAA should be sought for in the first place with materials difficult to dissolve, which may be considered macroscopically homogeneous but which are grossly too inhomogeneous for direct subsampling without extensive homogenization. Examples are materials from the waste recycling industries, e.g., plastics, shredded materials from electronic devices, domestic waste, waste from construction sites, etc. Also, the geological market segment might be interested in large sample INAA (with maximum length of 100 cm and maximum diameter of 15 cm), particularly for analysis of samples (rocks, drill-cores, as well as sediments) with inhomogeneously distributed depositions. In a later stage, research into localizing these inhomogeneities may be forecast as a logical next step.

Received for review March 23, 1995. Accepted October 23, 1995.[⊗]

AC950287W

[⊗] Abstract published in *Advance ACS Abstracts,* December 1, 1995.